Theor Chem Acc (2012) 131:1254
DOI 10.1007/s00214-012-1254-3

REGULAR ARTICLE

From atoms to biomolecules: a fruitful perspective

E. Cauët · T. Carette · C. Lauzin · J. G. Li · J. Loreau · M. Delsaut · C. Nazé · S. Verdebout · S. Vranckx · M. Godefroid · J. Liévin · N. Vaeck

Received: 17 April 2012 / Accepted: 26 June 2012

Abstract We present a summary of the research activities of the "Quantum Chemistry and Atomic Physics" theoretical group of the "Chimie Quantique et Photophysique" Laboratory at Université Libre de Bruxelles. We emphasize the links between the three orientations of the group: theoretical atomic spectroscopy, structure, and molecular dynamics and list the perspectives of our collaboration.

Keywords Electronic correlation · Relativistic effects · Isotopic effects · Multiply excited states · Hollow atoms · *B*-spline basis set · Charge transfer · Photodissociation · Radiative association

1 Introduction

The "Quantum Chemistry and Atomic Physics" theoretical group of the ULB "Chimie quantique et Photophysique" (CQP) Laboratory actively participated in the series of "Quantum Chemistry in Belgium" meetings since the very first one (Namur 1995). During almost forty years, the seniors of this group (JL, MG, and NV) pursued the tradition of their predecessor, Georges Verhaegen, in investigating methodology transfers from atomic physics to quantum chemistry and vice versa. Among these developments, one finds the "atoms-in-molecules" approach[1] [105] that was developed to estimate the electron correlation molecular energy from atomic correlation energies [49] or the "transition states" method with fractional occupation numbers [67] to calculate atomic transition probabilities. Another tradition of our laboratory that the authors maintained, together with their colleagues Michel Herman and Jean Vander Auwera from the high resolution spectroscopy experimental group of the same laboratory, is to benefit from the theory-experiment synergy, as initiated by the tandem Reginald Colin—Georges Verhaegen in their study of BeH [41].

The present research activities of the theoretical group fit three main fields: ab initio atomic and molecular structures and quantum molecular dynamics. Some of the research subjects merge expertise from two different fields. For instance, the investigation of molecular dynamics is achieved by developing both wave packet propagation techniques [110] and molecular structure methodologies [112]. Another example is the continuous quest for new approaches to take electron correlation into account [174] that remains, since the beginning of ab initio calculations, the key for an adequate description of atomic [21] and molecular structures and properties [107]. A number of our research projects have direct astrophysical applications, including the determination of accurate atomic oscillator strengths and the investigation of isotopic and nuclear

Published as part of the special collection of articles celebrating theoretical and computational chemistry in Belgium.

E. Cauët · T. Carette · C. Lauzin · J. G. Li · J. Loreau · M. Delsaut · C. Nazé · S. Verdebout · S. Vranckx · M. Godefroid · J. Liévin · N. Vaeck (✉)
Chimie quantique et Photophysique, Université libre de Bruxelles, 50, av. F.D. Roosevelt, CP160/09, 1050 Brussels, Belgium
e-mail: nvaeck@ulb.ac.be

M. Godefroid
e-mail: mrgodef@ulb.ac.be

J. Liévin
e-mail: jlievin@ulb.ac.be

[1] Not to be confused with the Atoms In Molecules (AIM) approach of the late Richard Bader [6].

Published online: 03 August 2012

effects [71], the characterization of molecules suspected in space [137], the determination of rotational intensities to predict molecular abundances [29], or the calculation of rate constants for charge transfer processes [168, 169]. Contributions within each field may thus be very diverse and include also the calculation of atomic electroaffinities [20], time-dependent photodissociation processes [114], or DNA stacking properties [32]. We have gathered here some examples of our works which have been presented at the QCB meetings for more than 15 years now.

2 Theoretical atomic spectroscopy

The ab initio calculations of atomic structures are often dictated by high resolution spectroscopy laboratory experiments or by astrophysical observations that require reliable atomic parameters for their interpretation. The spectacular increase of the spectral resolution during the last two decades, in all domains of the electromagnetic spectrum, forced the theoreticians to improve their models and computational tools to achieve the needed accuracy in their atomic structures and dynamical properties calculations. This applies not only to laboratory measurements but also to observational spectroscopy for astrophysics and astronomy thanks to high resolution spectrometers coupled to ground-based or space telescopes.

We illustrate in the present section the important role of high resolution atomic structure calculations through specific examples, keeping in mind for their selection, that they should be of interest for the quantum chemistry community.

2.1 The partitioned correlation functions approach

It has been known for many years that variational methods can be used for targeting specific correlation effects by tailoring the configuration space [70]. We proposed a new method that was successfully applied for describing the total energy of the ground state of beryllium [174]. Independent sets of correlation orbitals, embedded in "Pair Correlation Functions (PCFs), are produced from separate multiconfiguration Hartree–Fock (MCHF) calculations [60]. These non-orthogonal one-electron functions span configuration state function (CSF) spaces that are coupled to each other by solving the associated generalized eigenvalue problem. The Hamiltonian and overlap matrix elements are evaluated using the biorthonormal orbital transformations and efficient counter-transformations of the configuration interaction eigenvectors [122]. Using this approach, we demonstrated the fast energy convergence in comparison with the conventional SD-MCHF method optimizing a single set of orthonormal one-electron orbitals for the complete configuration space. Very recently, we moved to a more general approach renamed the "Partitioned Correlation Function Interaction" approach [175] that keeps the same PCFI acronym, but that is not necessarily restricted to a pair partitioning. This original method is currently tested on the ground and the first excited state of neutral lithium, not only for the total energy, but also through the expectation values of the specific mass shift and hyperfine structure operators and radiative transition probabilities, using different models for tailoring the configuration space. We clearly identified the "contraction effect" as the source of inaccuracy for properties more sensitive than the energy, due to the use of fixed PCF eigenvector compositions. A progressive decontraction, up to the uncontracted non-orthogonal configuration interaction limit case, efficiently solves the problem by restoring the needed flexibility in the wave function. Let us illustrate the approach on $1s^2\ 2p^2P^o$ of Li I for which the following four PCFs:

- the inner-shell ($1s$) double-excitations PCF,
- the inter-shell ($1s$, $2p$) single- and double-excitations PCF,
- the ($1s$, $1s$, $2p$) triple-excitations PCF,
- the inner-shell ($1s$) single-excitations PCF,

are built and optimized independently by the MCHF approach, keeping frozen the $1s$ and $2p$ orbitals from the HF solution. Each PCF brings its own basis of numerical orbitals, up to ($n = 10$; $l \leq 9$), in the "Uncontracted Partitioned Correlation Function Interaction"(UPCFI) eigenpair problem. The union of the four above PCFs reproduces the Complete Active Space (CAS) CSF expansion as far as the excitation families are concerned, but the variational richness of the one-electron basis is much larger than the one of the traditional CAS-MCHF calculation. Figure 1 illustrates the tremendous gain of our UPCFI approach compared with the CAS-MCHF method in the convergence pattern of the electric quadrupole hyperfine parameter b_q with respect to the size of the orbital active set(s). This parameter is defined as the following expectation value:

$$b_q \equiv \left\langle \Gamma LSM_L M_S \left| \sum_{i=1}^{N} 2C_0^{(2)}(i) r_i^{-3} \right| \Gamma LSM_L M_S \right\rangle , \qquad (1)$$

calculated with $M_L = L$ and $M_S = S$ [71]. The ket $|\Gamma LSM_L M_S\rangle$ defines the atomic state function and b_q represents the electric field gradient at the nucleus, produced by the electrons, interacting with the quadrupole moment of the nucleus, if any.

Even if the lithium atom is a three-electron system that can be described accurately by a single orthonormal

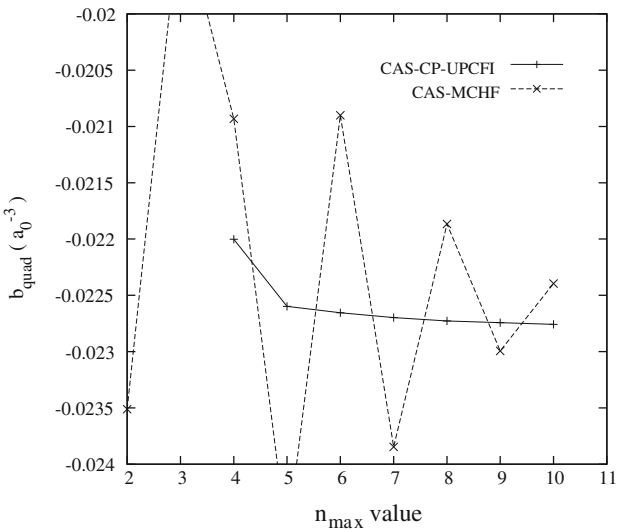

Fig. 1 Comparison of the CAS and uncontracted PCFI convergence patterns of the electric quadrupole hyperfine interaction parameter as a function of the size (n_{max}) orbital active set

orbitals set, the PCFI method leads to an impressive improvement in the convergence pattern of all spectroscopic properties studied so far [175]. For larger systems, it becomes quickly hopeless to saturate the space occupied by all electrons with a single common set of orthonormal orbitals, and the PCFI method is a promising approach that might become competitive with the coupled-cluster approach [8] for getting high-quality correlated wave functions. The present study constitutes a major step in the current developments of both ATSP2K and GRASP2K packages [61, 90] that adopt the biorthonormal treatment for estimating energies, isotope shifts, hyperfine structures, and transition probabilities.

2.2 Nuclear effects on the electronic structure

During the last decade, our research group focused on various nuclear effects in atomic structures and dynamics. A major contribution [17] is the theoretical calculations of hyperfine-induced transitions that occur due to the fact that the total electronic quantum number **J** allowed by the coupling $\mathbf{J} = \mathbf{L} + \mathbf{S}$ cannot be "good" enough due to the hyperfine coupling $\mathbf{F} = \mathbf{J} + \mathbf{I}$, where **I** is the nuclear spin. The resulting **J**-mixing opens new decay processes that may affect the radiative lifetimes [1, 89] and may be observed in astrophysics [18]. The estimation of these subtle interaction mechanisms requires the evaluation of the complete hyperfine interaction matrix in the basis of the atomic states involved, all described by highly correlated and relativistic-corrected wave functions. The evaluation of the hyperfine constants and their comparison with observation brings sometimes surprises. For hyperfine structures of ^{15}N and ^{14}N spectral lines observed in the near-infrared [85], we estimated ab initio hyperfine constants [91] that disagree completely with the experimental parameters obtained by fitting the observed hyperfine spectra [85]. We proposed a new interpretation of the recorded weak spectral lines [21] as crossover signals, producing a new set of experimental hyperfine constants in very good agreement with the ab initio predictions. This exemplifies the crucial role of theoretical atomic structure calculations in the interpretation of high resolution spectroscopy experiments.

Another property, often relevant in chemistry, that can be isotope-dependent is the electron affinity. The theoretical estimation of this observable constitutes a real challenge [121], due to the delicate energy balance between the neutral atom and its negative ion. In the last years, we developed elaborated correlation models to estimate the isotope shift on the electron affinity in carbon, oxygen, sulfur, and chlorine [11, 20, 22], mainly motivated by the interpretation of the microscopy photodetachment experiments [10]. The estimation of the mass shift contributions becomes arduous for heavy systems since the recoil operator should be relativistically corrected [148]. We develop the algebra and the computational tools for allowing their calculation in the full relativistic scheme [63].

2.3 Relativistic effects in light elements

The ab initio calculation of atomic structures in light elements and ionic species definitely requires special care in the description of electron correlation beyond the single-configuration (not always single-Slater determinant) Hartree–Fock (HF) approximation. Although relativistic corrections are expected to become important for high-Z systems, they cannot be neglected at the level of high resolution at low Z. Moreover, in some situations, relativistic effects can be much larger than expected. These surprises occur in the case of near-degeneracies of non-relativistic levels that strongly mix through relativistic operators such as the spin–orbit interaction. In the present contribution, we illustrate how relativistic corrections can be large in fluorine, despite its low atomic number ($Z = 9$). Table 1 reports the theoretical values of the magnetic dipole hyperfine constant A_J for $2p^4 3p$ that are estimated using elaborate single- and double-multireference MCHF correlation models [23], together with the experimental value [158] for $^2D^o_{5/2}$. The calculations are performed using the multiconfiguration Hartree–Fock (MCHF) and Dirac–Fock (MCDF) methods. In both non-relativistic and relativistic models, the set of many-electron states selected to form the total wave function is constructed systematically using the "single- and double-multireference" approach. In the framework of MCHF, the relativistic effects are taken into account either in the Breit–Pauli (BP) approximation

Table 1 Theoretical and experimental hyperfine interaction constants A_J (in MHz) for neutral fluorine

Level	MCHF	MCHF-BP	RCI	MCDF	Exp [158]
$2p^4(^3P)3p^2D^o_{5/2}$	2,040	1,691	1,679	1,666	1,746 (1.5)
$2p^4(^3P)3p^4P^o_{5/2}$	788	1,007	1,004	1,002	

using the MCHF orbitals or through relativistic configuration interaction (RCI) calculations, in which the non-relativistic one-electron basis is converted to Dirac spinors using the Pauli approximation [22]. Relativistic effects can play a significant role on the hyperfine structures. The good agreement between the MCHF-BP, RCI, and MCDF results illustrates that these three methods are valid to capture relativistic effects in a system like fluorine. The remaining discrepancies between experiment and theory arise from higher-order electron correlation and relativistic corrections.

2.4 Electron densities from relativistic wave function

Ruthenium, rhodium, palladium, osmium, iridium, and platinum, having similar physical and chemical properties, constitute the so-called "platinum group". By looking at the position of the last three of these elements ($76 \leq Z \leq 78$) in the periodical table, the chemist immediately realizes the expected complexity of their electronic structures. Following the lanthanides, however, the 4*f* shell is filled by 14 electrons and the valence structures $5d^N\,6s^M$ of Os, Ir, Pt mainly differ in the (N, M) occupation numbers of the 5*d* and 6*s* atomic subshells. Osmium combined with rhenium, ruthenium or iron, produces compounds that are known as ultra-hard and incompressible materials [45], with a high recognized potential in the cutting tools and abrasives industry [93]. Osmium has a ground state $[Xe]4f^{14}5d^6 6s^2\,^5D_4$ and the closeness of the valence shells with 4*f* makes an accurate description of its electronic wave function difficult to achieve. Moreover, relativistic effects are expected to be large with such a high number of protons [75]. We participate in the development of the computational atomic structure tools that are needed for getting a reliable description of such complex systems. Figure 2 displays the radial electron density $D(r)$ [12] of the osmium ground state, using three different models: HF, DF, and MCDF. The comparison between the HF and DF electron densities is striking and beautifully illustrates the importance of relativity for such a high-Z atom. But electron correlation is obviously crucial for many properties, although it is surprisingly difficult to visualize on the density itself [12]. The inset figure displays the magnified (×1,000) electron density difference between the single- and multiconfiguration pictures in the full relativistic scheme. The latter has been obtained by a single- and double-monoreference MCDF calculation, allowing one or two holes in the spectroscopic {4*f*, 5*d*, 6*s*} shells and adopting the {4*f*, 5*d*, 5*f*, 6*s*, 6*p*} orbital active set. As seen in this figure, the valence correlation induces some important reorganization of the electron cloud corresponding to an increase of the density in the outer region ($r > 1.5$ a_0). A new program (RDENS) [104], designed as a module of GRASP2K [90] and its most recent version as far as the angular Racah–Wigner algebra is concerned [92], is under construction, on the basis of the relativistic extension of [12]. The possibility of getting reliable ab initio electron densities of complex atomic systems in ground and excited states, taking correlation and relativity into account, opens new perspectives in the context of ab initio DFT and its role in electronic structure theory [9, 73].

2.5 From doubly to multiply excited states in hollow atoms

In collision processes between slow highly charged ions (HCI) and neutral atoms or molecules, multiple electron capture into excited states of the ions is possible. Double capture is by far the most studied experimentally and theoretically [161] mainly because of the possibility to also reach those doubly-excited states radiatively from the ground state [16, 62]. Note that this research area is still very active, as illustrated by the recent reinvestigation of our pioneer work [161] on radiative transition probabilities

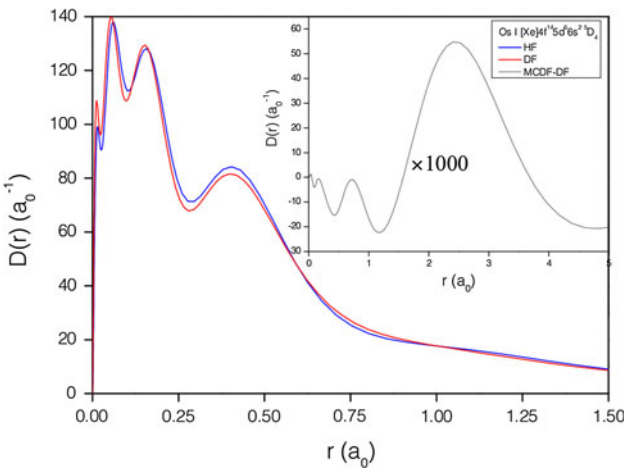

Fig. 2 Radial electron density $D(r)$ of the Os $[Xe]4f^{14}5d^6 6s^2\,^5D_4$ ground state

and Auger rates of the $1s^2 3\ell 3\ell'$ states in Be-like ions [147]. The capture of three electrons from the neutral target into triply excited states is also possible but the analysis of the resulting electron spectra is much more complicated due to the complexity of the Auger decay cascade of the triply excited states. Vaeck and Hansen [163, 166] have carried out the first theoretical studies of the triply excited $3\ell 3\ell' 3\ell''$ and $3\ell 3\ell' n\ell''$ of N^{4+} and $1s^2 3\ell 3\ell' 3\ell''$ of N^{2+} and of their decay properties. The lifetimes of those triply excited states are dominated by Auger decay and assuming a statistical population of the manifolds, the average lifetime is about two orders of magnitude smaller than the average lifetime of corresponding the doubly-excited states (2.1×10^{-15} s compared with 1.0×10^{-13} s).

Multiple charge transfer processes can also take place in collision experiments between highly charged ions and metallic surfaces. At a certain distance from the metal, due to the large Coulomb potential, the ion pulls electrons out of the conduction band of the metal. These electrons populate excited levels of the ion until it is totally neutralized, leaving inner-shells empty. The resulting hollow atom, for which most of the electrons are in high-n levels, decays via cascades of autoionization and radiative processes while staying neutral due to the pick up of additional electrons. After, the hollow atom hits the surface and is stripped of its highly excited electrons. The ion then enters the surface and again captures electrons in excited levels (see [170] and the references therein).

The first challenge in the interpretation of the experimental results is the determination of the Auger rates of hollow atoms in front of the metallic surface. For N^{6+} at 600 eV in front of an Au surface, Vana et al. [172] observed about 20 electrons ejected in 10^{-14} s while for Th^{71+} in front of an Au surface, Aumayr et al. [4] measured the emission of between 160 and 260 electrons depending of the velocity of the ion. Using a single configuration average approach (SCA), Vaeck and Hansen [162, 164, 167] have determined the decay properties of hollow atoms of the type $1s^{0,1,2} np^N$ with $n = 2$–7 and $N = 2$–6 in nitrogen and obtained a lifetime for the neutral species of the order of 3–6 $\times 10^{-16}$ s in good agreement with the experimental data. These results have been confirmed for other atomic systems. For more complex systems, Palmeri et al [123] have developed a group-diagrammatic summation method which allows the calculation of Auger rates for configurations of the type $6f^N$ in $Th^{(44-N)+}$. Finally, the statistical properties of Hollow nitrogen have been investigated in the framework of the Random Matrix Theory by Vaeck and Kylstra [171].

When the ion enters the surface, lower energy levels start to be populated giving rise to interesting structures in the electron spectra. For N^{6+} colliding on a Ni(110) surface [3], the LMM and KLL structures have been partially interpreted using theoretical results [78]. The comparison between the electron spectrum resulting from the collision of N^{6+} and N^{7+} reveals three-electron Auger processes of the type K^2L^2L in which two electrons are stabilized while one is emitted [59]. The calculation of the decay rate of these processes is dominated by the non-orthogonality between the wavefunctions of the initial and final states [165].

Multiply excited states are characterized by very large configuration mixing which govern their decay properties. We hope that some of the methodology developed to study hollow atoms can open new perspectives for the calculation of complex molecular spectra involving autoionizing states or for the study of ion-pairs (heavy Rydberg) states [138] that will start soon in our laboratory.

3 Bridging atomic physics and quantum chemistry

3.1 Brillouin's theorem

We put a lot of effort in clarifying the connection between the Brillouin–Lévy–Berthier and Brillouin–Bauche–Labarthe–Froese Fischer theorems [69], leading to an interesting tool for analyzing the variational content of molecular wave functions [106]. Regarding Brillouin's theorem as a property of the Hartree–Fock wave function, one can use it to test the quality of the converged solution [68]. The Hartree–Fock problem for the general open-shell f^N case was solved by Gaigalas thanks to the Vilnius angular algebra [64]. In collaboration with Gaigalas, we proceeded to such systematic tests along the lanthanides and actinides for assessing the reliability of the code. This brings us to some mysterious discoveries: all Brillouin matrix elements that should be strictly zero for the converged HF solution are strictly zero. However, many other zeros appear as well, and these are still not understood despite our search in finding hidden symmetries within the quasi- and/or iso-spin formalisms.

3.2 The treatment of one-electron non-orthogonalities

For years, we faced the huge problem of dealing with radial non-orthogonalities arising from the independent optimization of the states involved in transition amplitudes, when using the Wigner–Fano–Racah algebra [56] for evaluating the matrix elements. The biorthogonal transformation algorithm developed by quantum chemists [115] was the key, after some necessary adaptation to the SO(3) spherical symmetry [122], to keep the advantages of the irreducible tensorial approach. These tools are now implemented for all one- and two-body operators in both the non-relativistic and relativistic packages [74] and are intensively used not

only for the estimation of accurate transition probabilities, but also for energy differences and other properties as explained above in the PCFI section.

Bridging atomic physics and quantum chemistry is a rich inspiration source for new developments. Our recent work on the analysis of atomic physics calculations with methods from Quantum Chemistry [13] follows the same aim.

3.3 *B*-spline basis sets

B-splines are positive L^2 integrable piecewise polynomials of order K defined on a interval [0,R] from a recursive relation. *B*-splines have been used intensively in atomic physics to describe both the bond spectrum and the continuum of energy of atomic systems. One of the essential properties of the *B*-spline basis sets is their "effective" completeness which allows the entire spectrum, including the continuum states, to be replaced by a pseudospectrum containing only a finite number of states. The pseudospectrum is constructed in such way that the low-lying states represent correctly the low-lying bound states of the real spectrum with the remaining pseudostates representing the remaining bound and continuum spectrum [76].

Using a truncated diagonalization method with these *B*-spline basis sets, we have calculated the decay properties of all doubly- excited $4\ell4\ell'$ and $4\ell5\ell'$ states of O^{6+} and Ne^{8+} populated during collisions between Ar and O^{8+} or Ne^{10+}, respectively [79, 80]. We have determined the degree of radiative stabilization of these doubly-excited states and compared it with the experimental results.

We took advantage of the effective completeness of the *B*-splines to predict the electronic rearrangement resulting from the β decay of ^{6}He and $^6He^+$ in the framework of the sudden approximation [178] and by taking into account the recoil effects [179]. The shake off (ionization) probability of $^6Li^{2+}$ has been very recently measured in GANIL using a specially designed recoil ion spectrometer. This first measurement of an electron shake off following a β decay is in excellent agreement with our simple sudden approximation calculation [118].

The idea of using *B*-spline basis sets for the representation of vibrational molecular wave functions emerged rapidly. For a Morse potential and a two-dimensional Hénon–Heiles potential, we have assessed the efficiency of the *B*-splines over the conventional DVR (discrete variable representation) with a sine or a Laguerre basis sets [50]. In addition, the discretization of the vibrational continuum of energy when using the Galerkin method allows the calculation of photodissociation cross-sections in a time-independent approach.

The photodissociation of the molecular oxygen by UV solar radiation is the first step in the ozone-making reaction sequence

$$O_2 + h\nu \rightarrow O(^3P) + O(^3P)$$

$$O(^3P) + O_2 + M(M = O_2, N_2) \rightarrow O_3 + M$$

In the lower stratosphere, 90 % of the O_2 photodissociation results from transitions from the ground state $X^3\Sigma_g^-$ to the vibrational continua of the $A^3\Sigma_u^+, A'^3\Delta_u$ et $c^1\Sigma_u^-$ Herzberg states. Using a set a spectroscopic constants [87], we have constructed the RKR potential energy curves for the A, A′, c, and X states. The vibrational pseudospectra for all J values of these states have been obtained using 260 *B*-splines of order 13. The total cross section obtained in this work is compared to the available experimental and theoretical data in Fig. 3.

Finally, a *B*-spline method has also allowed the evaluation of the radiative decay probabilities of the six vibrational levels of the metastable $a^3\Sigma^+$ state of HeH^+. The transition $a^3\Sigma^+ \rightarrow X^1\Sigma^+$ is spin-forbidden, but acquires intensity through spin-orbit interaction with the singlet and triplet Π states [111].

4 Ab initio characterization of molecular structures

The evolution over the last decades of molecular ab initio calculations followed the spectacular methodological and

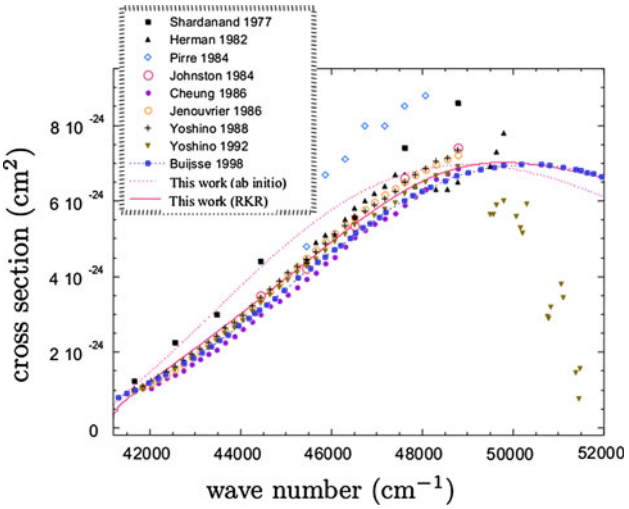

Fig. 3 Total photodissociation cross section for O_2 in the Herzberg states. "This work (ab initio)" corresponds to the use of ab initio potential energy curves and "This work (RKR)" to the use of RKR potentials constructed on the experimental data [87]. Comparison is made with the works of Shardanand and Prasad Rao [149], Herman and Mental [83], Pirre et al. [129], Johnston et al. [88], Cheung et al. [37], Jenouvrier et al. [86], Yoshino et al. [184], Yoshino et al. [185] and Buijsse et al. [19]

computational developments depicted in Sect. 2 for atomic calculations. It not only concerns the improvement of the methods of calculations for taking electron correlation and relativistic effects into account, and for treating excited states, but also the developments related to the nuclear degrees of freedom in molecules, like the handling of multi-dimensional potential energy surfaces [177] and the treatment of non-adiabatic couplings [53]. It also follows the increasing power of computer clusters allowing more accurate calculations on systems of increasing size. The size of a microscopic system is of course a subjective quantity, depending on both the number electrons and nuclei, the latter being equal to one for atoms and ranging from two to infinity for molecules, from diatomics to polymers. It is usually admitted that systems of two atoms or more belong to the world of "Chemistry", and specific theoretical developments are dedicated to different kinds of chemical objects. Application of Quantum Chemistry to biomolecules will be illustrated in Sect. 6 We will focus in this section on small molecules of atmospheric or astrophysical interest, for which a theoretical support to high resolution spectroscopy experiments is needed. As in the atomic case, we will highlight the theoretical efforts made for converging the calculated properties to experimental accuracy.

4.1 Determination of accurate molecular equilibrium properties

We first present some recent results on small hydrocarbons: methane, acetylene, and the methyl cation CH_3^+. Benchmark calculations have been performed on the determination of the equilibrium geometries of these species in their ground electronic state. These systems identified in numerous planetary atmospheres and interstellar medium present a renewed astrophysical interest [66, 102] and are extensively studied in high resolution laboratory experiments [14, 51].

The methyl cation CH_3^+ is involved in the interstellar reaction $C + H_3^+ \rightarrow CH^+ + H_2$, under study in our group [47].

Table 2 illustrates the convergence pattern up to the complete basis set limit (CBS) of the equilibrium CH bond distance in the ground $^1A_1'$ state (D_{3h} symmetry). Convergence is studied as a function of the extension (n = D, T, Q, 5 and 6) of the hierarchical aug-cc-pVnZ [54, 94] (AVnZ in short) and aug-cc-pCVnZ [182] (ACVnZ in short) basis sets. All calculations were performed using the internally-contracted multireference configuration interaction method (IC-MRCI) [95, 180] implemented in the MOLPRO program suite. The active spaces defining the multireference treatment coincide with the valence space for AVnZ calculations and with the full-(core + valence) active space for ACVnZ ones. All MRCI energies were corrected for Davidson's contribution for unlinked clusters [97]. CBS-extrapolation has been carried out on the energy, and not on the bond length value itself, as already done in other works [131]. Energies were extrapolated at each of the geometries scanned by the numerical derivative algorithm and numerical gradient optimizations have been applied to the extrapolated energies, as implemented in the MOLPRO code [181]. Extrapolations were separately applied [57, 173] at each geometry for the reference CASSCF energy and the dynamical correlation energy, using a simple exponential function [57] and a n^{-3} two-parameters form [81] respectively. The results show that, referring to the CBS value, one reaches the 0.1 pm accuracy at quintuple zeta level and that the introduction of the core and core-valence correlation (ACVnZ calculations) induces a contraction of the CH bond by 0.15 pm. Let us also note the agreement between IC-MRCI/AVnZ(CBS) and CCSD(T)-F12/VnZ-F12 frozen core results [46], with a faster convergence of the latter due to the use of explicit correlation.

In a similar study carried out on the ground electronic state of acetylene [107] at CCSD(T) level of theory, we found that the contribution of core electrons to the correlation energy decreases the CH equilibrium bond distance by a comparable amount (0.13 pm) as for CH_3^+. A similar contraction effect, but more pronounced (0.27 pm) as expected, is observed for the CC bond distance. The convergence of the ab initio equilibrium geometry to experimental accuracy was further addressed by also evaluating the effects of explicit triple and quadruple excitations (−0.014 and +0.042 pm for CC and CH, respectively), scalar relativistic corrections (−0.016 and −0.027 pm, respectively) and diagonal Born-Oppenheimer corrections (DBOC) (+0.013 and +0.003 pm respectively). Let us note that the DBOC calculations make use of the biorthogonal algorithm [115] cited in Sect. 3 The final ab initio values for both bonds, obtained by combining all mentioned contributions, are underestimated by about 0.02 pm with respect to the experimental values. Note that the latter were determined from a large number of ro-vibrational lines recorded for five isotopologues, providing thus a quite unique case for obtaining very accurate equilibrium parameters. These experimental values differ however from semi-empirical ones, also determined in Ref. [107] and based on results for ten isotopologues. Note also that non-adiabatic corrections are not taken into account in usual spectroscopic models. Above comparisons thus give an order of magnitude of the attainable accuracy on equilibrium geometries not only from ab initio calculations but also from experimental data.

Table 2 Convergence to CBS of the equilibrium CH bond length (in Å) of the ground electronic state of CH_3^+

n	D	T	Q	5	6	CBS
IC-MRCI/AV*n*Z	1.10380	1.09094	1.08951	1.08903	1.08898	1.08879
IC-MRCI/ACV*n*Z	1.10269	1.08967	1.08806	1.08758	1.08750	1.08729
CCSD(T)-F12/V*n*Z-F12 [46]	1.08913	1.08905	1.08875	–	–	–

Extensive calculations were also performed on methane [25–29], with the goal to predict the rotation–vibration spectrum which is of particular interest for evaluating methane abundance in planetary atmospheres. Our most recent results use an accurate potential energy surface calculated at the CCSD(T)/ACV5Z level of theory [119] and a dipole moment surface that we calculated at the IC-MRCI/ACV5Z level. The vibrational Schrödinger equation has been solved variationally, and perturbation theory was used to calculate the rotational spectrum of the ground vibrational state [29]. Note that the variational method developed for solving the vibrational problem, the vibrational mean field configuration interaction method (VMFCI) [26, 27], is directly inspired from electronic ab initio SCF/CI theory. The rotational spectrum calculated in that way is in very good agreement with the one recently recorded at the SOLEIL synchrotron [14] and with the atmospheric HITRAN database [142]. Note that part of this success comes from the accurate equilibrium geometry ensured by the use of the ACV5Z basis set in highly correlated calculations. As for the hydrocarbon systems mentioned above, the effect of core and core–valence correlation is to reduce the CH bond, by 0.02 pm in the case of methane.

4.2 Excited electronic structure of transition metal containing diatomics

Transition metal containing molecules have a potential astrophysical importance [109] and present an interest in catalysis and organometallic chemistry [24]. Numerous diatomic molecules MX made of a transition metal atom M and a second or third row atom X have been studied in laboratory using Fourier transform emission spectroscopy. Such experiments produce high resolution spectra covering a wide spectral range (typically from 0 to 25,000 cm^{-1}) and exhibit an intricate superposition of ro-vibrational bands. These spectra can usually not be assigned without a theoretical support. The complexity comes from the existence of many electronic states splitted by spin–orbit coupling and perturbed by non-adiabatic interactions. It also comes from the dense ro-vibrational structure conditioned by Franck–Condon factors and Hund's case angular momentum couplings. The electronic structure of the transition metal atom participating to the molecule formation is clearly at the origin of this complexity. As pointed out in Sect. 2, the transition metal is subject to relativistic effects and to important correlation effects arising from its valence shell $(n+1)s^N\, nd^M$, coupled to the $ns^2\, np^6$ inner-shells and possibly to the 4*f* shell for sixth row elements. The high degeneracy of the low-lying transition metal atomic states and their splitting in the molecular $C_{\infty v}$ environment explain the high density of molecular electronic states in the spectral energy window. Providing a reliable energy scale of the molecular electronic states lying within this window is a challenge for ab initio calculations, but is a prerequisite to any spectroscopic assignment. Our group has provided a theoretical support for assigning the spectra of many transition metal containing diatomics recorded by Bernath's group (see for instance [132–135, 137]). The quantum chemistry approach we adopted for such systems is the CASSCF/IC-MRCI method, well adapted to excited state calculations with efficient account of electron correlation. Quasi-relativistic pseudo-potentials and corresponding basis sets are moreover used for the transition metal atom [2].

In many cases we found that the succession of electronic states drastically changes within an isovalent MX series. We showed for instance that the ground state of (IVb)-group chlorides changes from $^4\Phi$ to $^2\Delta$ from TiCl to HfCl, both states being quasi-degenerated for ZrCl [136]. We also showed that the low-lying quartet excited states are inverted in ZrF [152] with respect to ZrCl.

A similar situation is illustrated in Fig. 4 in the case of the diatomic nitrides of ruthenium, osmium, and iridium (transition metals of the "platinum group"), studied independently [132–134]. This choice of atoms for illustrating this topic rejoins the atomic physics interest in our group, pointed out in Sect. 2. The Figure shows that the low-lying electronic structure of the isovalent Ru and Os atoms can be described in terms of 4 main electronic configurations, labeled from (A) to (D), but that configurations (B), (C), and (D) are pushed to higher energies in OsN, with as a result a change of ground electronic state and an extension of the energy scale by more than 10,000 cm^{-1}. The reason for these changes can be interpreted in terms of the balance of correlation effects within the interacting shells (the natural orbitals of the IC-MRCI calculations of course move accordingly). Going from OsN to IrN corresponds to the addition of a single electron, which can tentatively be associated with different molecular orbitals from the analysis of the wave functions.

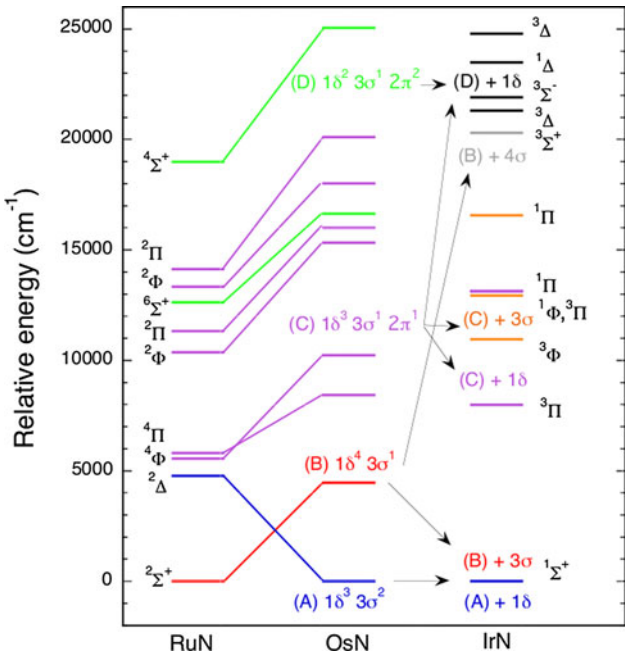

Fig. 4 Energy level diagram of the electronic states of RuN, OsN and IrN, from IC-MRCI calculations. *Colors* are used to mark states arising from the same configuration

4.3 Intermolecular potential energy surfaces of acetylene–rare gas complexes

High resolution infrared spectroscopy experiments carried out in our lab on acetylene-containing complexes motivated us to carry out large scale ab initio CCSD(T) calculations to support experimental results. Complexes are formed in a supersonic expansion allowing the detection of the complexes by means of cavity ring-down spectroscopy [52]. Accurate intermolecular potential energy surfaces (IPES) have been calculated for interpreting the $\nu_1 + \nu_3$ spectra of acetylene–rare gas complexes, the rare gas atom being argon, krypton, and xenon [101]. The spectra of the former two complexes have been studied experimentally [99, 100] but further theoretical help is needed for detailed analysis. IPES are defined by two coordinates R and θ, defining the Jacobi vector pointing from the center of mass of the acetylene moiety to the rare gas atom. Interaction energies were corrected for the basis set superposition error by means of the counterpoise approach [15]. Extensive test calculations have shown that the CCSD(T) method using all-electron AVQZ basis sets [54, 94] augmented by a set of (3*s*3*p*2*d*1*f*) midbond functions [157] provided interaction energy values close to the corresponding CBS limit. For krypton and xenon, multiconfigurational Dirac–Fock relativistic core potentials and corresponding AVQZ basis sets were used [126]. Table 3 illustrates the spectacular influence of both the correlation energy and the basis set on the stability of the global minimum of the acetylene–Kr complex. The positive values of the interaction energy at Hartree–Fock level shows how dispersion correlation effects determine the complex stability. Also note the importance of the basis set effect at CCSD(T) level, related to the description of the dispersion energy. The contributions of the scalar relativistic effects to the interaction energy have been evaluated to 1 and 2.3 % for acetylene–Kr and acetylene–Xe, respectively [101].

Table 3 Convergence to CBS of the interaction energy ΔE (in cm^{-1}) at the global minimum geometry of the acetylene–Kr complex

Method	Basis set	ΔE
HF	CBS(AV*n*Z + midbond)	+147.14
CCSD(T)	AVQZ	−141.39
CCSD(T)	CBS(AV*n*Z)	−153.11
CCSD(T)	AVQZ + midbond	−149.73

5 Non-adiabatic wavepacket molecular dynamics

Over the past decade, the Laboratoire de chimie quantique et photophysique of the ULB and the Laboratoire de chimie physique of the Université de Paris 11, Orsay have collaborated on the development of a strategy for the calculations of charge transfer cross-sections in ion-atom collision [110, 113, 168, 169],

$$A + B^{q+} \rightarrow A^{++}B^{(q-1)+}$$

This approach is based on a molecular description of the reaction in which the colliding particles engage in the reaction by the entrance channels corresponding to potential energy curves of the diatomic molecule AB^{q+}, form an unstable molecular bond, and dissociate into different exit channels. This method allows the use of conventional quantum chemistry program libraries for the calculation of the potential energy curves and of the coupling matrix elements which couple the entrance and exit channels in inelastic scattering. One of the expertise of the ULB team is the ab initio calculation of these time-independent parameters [112]. The dynamics of the nucleus is treated quantum mechanically, that is, the most appropriate approximation for low or very low collision energies encountered in the problems of interest in this proposal, by time-dependent wave packet propagation. For each collision energy, a Gaussian wave packet is prepared in the entrance channel and propagated on the coupled channels using the split-operator algorithm or the Chebyshev method. The cross-sections are extracted from the amplitude of the wave packets on the different exit channels at large internuclear distances using various numerical techniques such as the spectral projection or based on the properties of the flux operator [7].

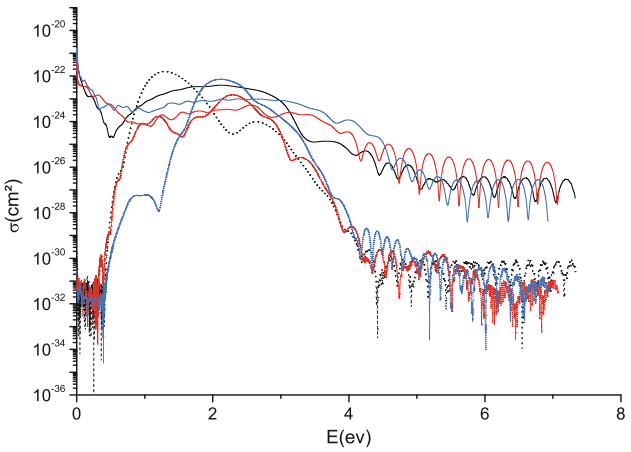

Fig. 5 Radiative association cross-sections of He($1s3s^3S$) + H^+ (*black curves*), He($1s3p\ ^3P^o$) + H^+ (*red curves*), and He($1s3d\ ^3D$) + H^+ (*blue curves*) toward the $b^3\Sigma^+$ state of HeH^+ with (*full lines*) and without (*dotted lines*) taking the vibrational dependence of the cross-sections into account

One of the advantages of time-dependent simulations is that they easily allow for the addition of the effect of an electromagnetic field on the dynamics, allowing the calculation of photodissociation and radiative association cross section for systems with one [151, 114] or two [5, 98] nuclear degrees of freedom. One example is the determination of the photodissociation and the radiative association cross-sections and rate constants of the molecular ion HeH^+, a species of particular interest in astrochemistry. We more specifically studied the difficulties met in extracting the cross-sections in systems which contain a very large number of coupled electronic states using a time-dependent method. Figure 5 shows the radiative association cross section of He($1s3s^3S$) + H^+, He($1s3p^3P^o$) + H^+, and He($1s3d^3D$) + H^+ toward the $b^3\Sigma^+$ state of HeH^+.

It is also possible to optimize the pulse of the laser to reach specific molecular states or reaction products, that is, quantum control. Orsay' LCP has a large expertise in that field and its application to chemical reactivity [120] and quantum computing [156]. In our approach, the control pulses are designed either by optimal control theory, by local control or by STIRAP (Stimulated Raman Adiabatic Passage). The most recent applications have been devoted to the implementation of quantum gates using states of cold diatomic molecules: using optimal control theory, we numerically implemented classical and quantum algorithms on hyperfine states of neighboring polar molecules in an optical trap. The prospect of operating intermolecular gates opens possibilities toward scalability and hyperfine states were shown to be good candidates for qubit encoding [124, 176].

6 Quantum chemical calculations of biomolecules and their environment

Research in theoretical and computational chemistry is also being carried out in our group with a special emphasis on applying quantum mechanics methods to molecular biophysics and chemical reactions in condensed matter. Dynamics and electronic structure theory calculations are being performed on large and complex systems to contribute to a better understanding of a variety of issues associated with biological and chemical structure and reactivity. In particular, a large effort of our research is being devoted to the elucidation of the mechanisms responsible for the radiation damage in DNA. Dynamics calculations are also being carried out with a special focus on the analysis of enzyme reactions and reactions occurring at the metal–solution interface. In addition, we are expanding our interests into molecular mechanics and combined quantum mechanical and molecular mechanical simulations of macro(bio)molecular systems. In this section, we summarize the contributions of modern quantum chemical calculations to the determination of the electronic properties of DNA bases, isolated or embedded in base clusters. In particular, the calculations discussed concern the characterization of the molecular energy levels and potential energy surfaces, which shed light on ionization and charge migration along DNA molecules. We mainly consider the estimation of key parameters, such as ionization energies (IEs) of DNA bases, which govern the charge injection into DNA. We also discuss the mechanisms of charge migration over stacked DNA bases and selected calculations performed on metal complexes used as DNA intercalators. Finally, the influence of the DNA environment and its effect on the IE quantities are described.

6.1 Isolated DNA bases and DNA base clusters

When trying to elucidate the effects of ionizing radiation on DNA, knowing the electronic structure of DNA is imperative. Indeed, detailed information about electronic properties of the DNA components will ultimately provide a fundamental understanding of the electronic factors that influence site-specific or sequence-specific radiation attack on DNA. Ab initio quantum mechanical calculations bring realistic descriptions of the Born–Oppenheimer potential energy surfaces of the neutral and cationic electronic states that govern the studied ionization properties of the DNA constituents. They also determine structures and relative energies of the relevant stationary points (minima and saddle points) on the corresponding potential energy surface and reveal the reaction pathways connecting them. A fundamental advantage is that quantum mechanical

calculations reveal a direct relation between structure and energies, which is close to impossible to achieve via experimental approaches. On the monomer level, that is, isolated nucleobases, the application of quantum mechanical calculations has proven to be a powerful tool [58, 77, 96, 116, 150] because the interpretation of the experimental results is not yet complete owing to the frightening task of extracting contributions of numerous tautomers and conformers that can be produced under the experimental conditions (especially in the case of guanine and cytosine) [58, 96, 117, 160, 187]. Moreover, the advanced quantum mechanical calculations have been used as predictive tool for systems where no relevant experiment exists, such as hydrogen-bonding and π-stacking of nucleobases [35]. Thus, the improvement of quantum mechanical calculation techniques, together with the increase in computing power, allows today for precise analysis of ionization properties of clusters of DNA bases "in complete isolation", providing a detailed understanding of the intrinsic features of such systems. However, the application of the above-mentioned quantum mechanical calculations is far from being trivial given the ionization properties to be calculated and the size of the molecules and the interactions of interest. Stacking and H-bond interactions between nucleobases are still a challenge for quantum mechanical methods, the details of this have been reviewed in Refs. [31, 139, 154, 153]. The choice of the level of calculation well adapted to the studied problem is crucial.

While the ionization of isolated DNA bases and H-bonded base pairs has been studied extensively (see Ref. [35] and references therein), only a few ab initio IE calculations on π-stacked bases have been reported. Indeed, whereas the qualitative features of ionization of stacked systems, that is, the lowering of IE and the dependence of hole delocalization on the relative orientation of the fragments, can be easily explained by an electrostatic model [130] and simple molecular orbital analysis, as has been done by Sugiyama and Saito [143–146, 155, 186], the quantitative predictions are much more challenging. The influence of stacking interactions on guanine IE has been examined by employing single- and double-stranded model systems consisting of stacked guanine bases in orientations that occur in the standard B-form of DNA [30, 31, 36, 130, 143, 144, 155, 186]. Figure 6 summarizes the recent results concerning pure guanine single-strand stacked clusters. These include MP2 estimates using the polarized 6-31G(2d(0.8,0.2)) basis set. In this case, the geometries of the systems are not optimized and the values are vertical IEs. Stacking interactions in the GG dimer are found to reduce the vertical IE by 0.4 eV. A similar effect of stacking interactions on IEs has been reported in the case of the benzene dimer (0.53 eV) [127, 128] and the uracil dimer (0.34 eV) [72]. The IE lowering by stacking interaction is further confirmed for three, four, five, and six consecutive stacked guanines, in which the IE gradually drops with increasing number of nucleobase. The IE difference between dimer and trimer is 0.1 eV while the IE change between trimer and tetramer is larger (0.6 eV). In order to evaluate the IE sequence dependence, IEs were also estimated for different sequences of stacked DNA bases, in particular the human telomere sequence (TTAGGG) [36], which is essential for chromosomal stability and integrity, a function important for DNA damage. As depicted in Fig. 6, ionization energy calculations show that the G-rich human telomere sequence is particularly prone to oxidation and can act as a profound hole trap as deep as a sequence of five consecutive guanines. These calculations thus support the previously reported hypothesis of the protection of genes from oxidative damage by telomeric overhangs [82]. A molecular orbital analysis has been done explaining how unique the human telomeric sequence is and how modifications in the sequence are expected to induce changes in the electronic structure, with concomitant increase of the ionization energy.

Due to charge transfer between DNA bases, the chemical damage in irradiated DNA often occurs at sites other than where the original ionization takes place. For these reasons, the elucidation of the mechanisms responsible for the charge transfer phenomena in DNA is also a grand challenge in the current research on the oxidative damage of DNA. A key structural element, which determines the charge transfer properties of DNA, is the array of the π-stacked base pairs [159, 183]. DNA-mediated charge transfer has proven to be gated by base motions and, as such, to be sensitive to DNA conformation and stacking, with only certain base conformations being charge transfer active. A key theoretical result of our research has been the characterization, in gas phase, of very specific conformations of an ionized DNA stacking of two consecutive guanines, the most easily oxidized nucleic acid base, required for charge transfer to occur [32]. Our analysis relied on high-level multiconfigurational ab initio calculations: state-averaged CASSCF/MRCI and RASSCF/RASPT2. The ground and first two excited states of the radical cation have been characterized and the topology of the corresponding potential energy surfaces has been studied as a function of all intermolecular geometrical parameters. Relative translational motions of both guanines in their molecular planes have been demonstrated to govern the charge migration between the two bases. The reaction path describing the charge transfer from one guanine to another has been predicted. Five stationary point conformations of ionized guanine pairs (see Fig. 7) have been characterized corresponding to three minima (M1, M2 and M3) and two saddle points (S1 and S2). The corresponding relative energies with the percentages of the positive

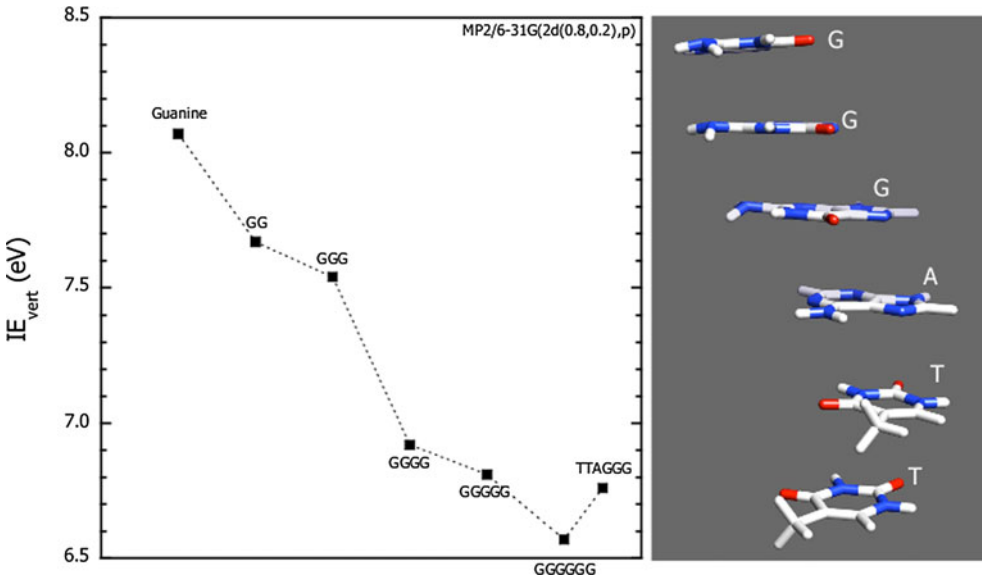

Fig. 6 Vertical IEs (in eV) of B-form stacked contiguous guanines and the 5′-TTAGGG-3′ human telomere sequence

charge, calculated for each stationary point, on G5′ and G3′ are presented in Fig. 8. In addition, we have extended our study to a stacked sequence of three guanines isolated (GGG) and in interaction with the amino-acid arginine (GGGArg). The results of the calculations performed on these trimer geometries are promising and very exciting as they show that the charge transfer, first, proceeds in a multi-steps fashion, from one base to another, across the trimer and, second, may be modulated by a H-bond/cation-π stair motif, as the one found in GGGArg. These motifs are recurrently found at protein/DNA interfaces [140]. They can thus be viewed as stabilizing the stationary point conformations and modulating the charge transfer by the introduction of a positive charge in the vicinity of the guanine stack [141].

6.2 DNA intercalating complexes

In typical experiments designed to study the charge transfer in DNA, a donor and an acceptor of these charge carriers are intercalated in the stack of the DNA bases or chemically attached to the phosphate–sugar backbone. For a properly chosen donor and acceptor species, such chemical modifications enable the generation of holes under irradiation of the sample by light due to the removal of an electron from the nucleobase to the photoexcited donor. In the burgeoning area of DNA intercalation studies, transition metal intercalators have been a rich source of experimental data for decades and, in this context, the Ruthenium derived compounds have been extensively used. The rich chemical and structural diversity of the Ru(II) compounds has provided the biological chemists with a range of chemical, luminescent and photochemical probes to study DNA but also to potentially open new routes to diagnostic and therapeutic agents for various diseases. Indeed, when the photo-induced electron transfer is efficient, it has been shown experimentally that this may correlate with the single-strand cleavage of plasmid DNA. Extensive research has been performed on Ru(II) complexes in the presence of nucleic acids in Prof. A. Kirsch-De Mesmaeker′s research group [48, 55, 84, 103]. Recently, Prof. A. Kirsch-De Mesmaeker and Prof. M. Luhmer showed, for the first time, that the photoreaction of $[Ru(tap)_3]^{2+}$ and $[Ru(tap)_2(phen)]^{2+}$ with guanosine-5-monophosphate or *N*-acetyl-tyrosine gives rise to ^{1}H photo-CIDNP signals [125], that is, non-Boltzmann nuclear spin state distributions that has been detected by NMR spectroscopy as enhanced absorption or emission signals. However, the interpretation framework must be confirmed. In order to validate the experimental predictions, Density Functional Theory (DFT) calculations can be performed. These calculations are based on the determination of the electronic structure of the mono-reduced form of Ru(II) complexes in gas phase and aqueous solution. Recently, some of us showed that the electron spin density and the isotropic Fermi contact contribution to the hyperfine interactions with the ^{1}H nuclei agree remarkably well with the observed ^{1}H photo-CIDNP enhancements [34]. Thus, combined photo-CIDNP experiments and DFT calculations open up new important perspectives for the study of polyazaaromatic Ru(II) complexes photoreactions.

6.3 Influence of the DNA environment

As described in the earlier sections, ab initio studies have contributed to a fundamental understanding of the intricate effects of the different elements of the DNA environment, including bonding in nucleotides, H-bond and stacking

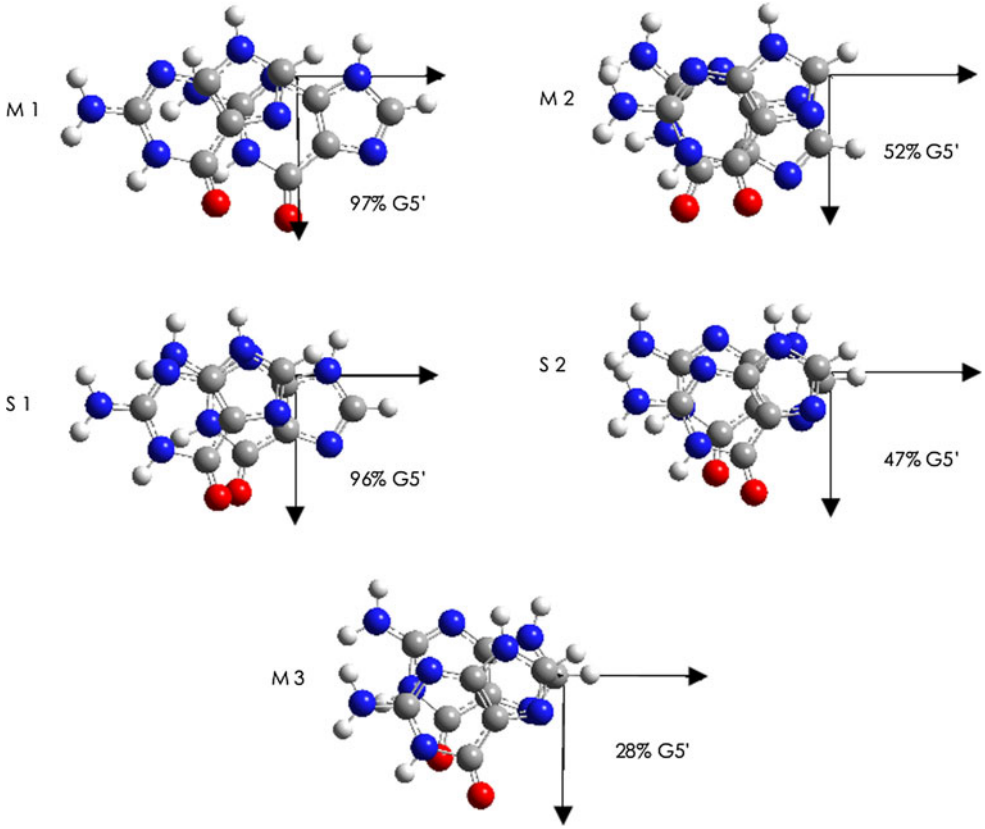

Fig. 7 Conformations of the ionized stacked cluster GG corresponding to the five stationary points (M for minimum and S for saddle point). The percentages of the positive charge on the guanine G5′ are also indicated

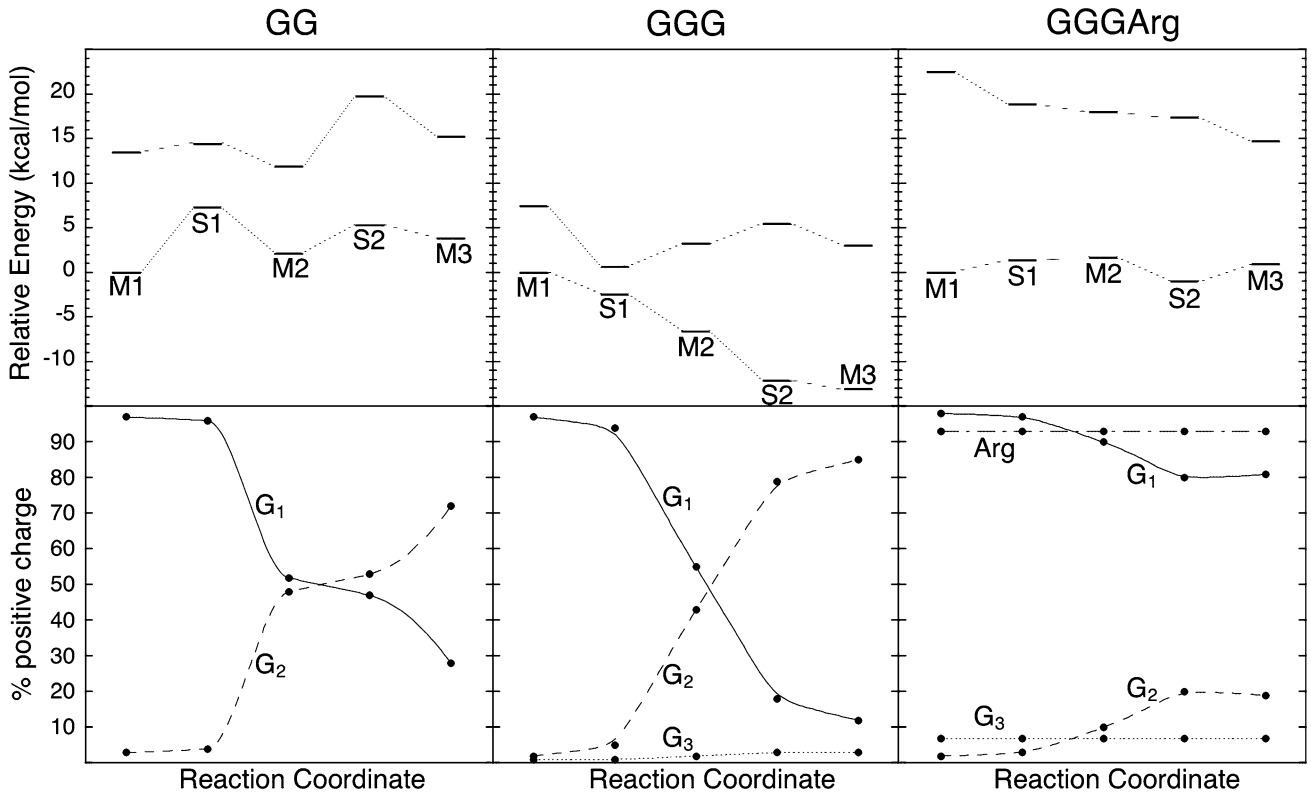

Fig. 8 *Top* relative energies (in kcal/mol) of the ground and first excited states, computed at the RASSCF/RASPT2/6-31G(d(0.2)) level of theory, for the ionized stacked clusters GG, GGG and GGGArg. The energies for the five optimized conformations represented in Fig. 7 have been calculated. *Bottom* percentages of the positive charge on each component of the clusters calculated for the ground state

Table 4 Results of CCSD(T)/aug-cc-pVDZ gas phase and QM/MM calculations of vertical IEs of DNA bases (in eV)

Nucleobase	Gas phase	QM/MM	Δ
Guanine	7.90	11.09	3.16
Adenine	8.23	11.55	3.32
Cytosine	8.65	11.98	3.33
Thymine	8.98	12.33	3.35

interactions between DNA bases but also solvation [38–40, 42–44, 125], on the IEs of each of the bases. However, it is important to have a global vision of the various aspects of the environmental effects to extrapolate these observations to predict the electronic properties of DNA bases in a biologically relevant aqueous environment. The DNA bases embedded in the DNA helix experience very special electrostatic interactions with the solution structure outside the helix. Indeed, a long-range solvent structure is created by the presence of the negatively charged phosphates of the backbone and the positive counterions. All these effects can cause important changes in the electronic structure of the DNA bases and the next step is thus to ask what the electronic properties of DNA bases are if we take these into account. The modeling of the DNA solution is an important challenge with many thousands of participating atoms. While significant progress is being made in the development of quantum chemical approaches applicable to large systems, it is clear that to treat complex biological systems such as DNA we still need to integrate different computational methodologies with diverse accuracies and cost. The goal of our research is to gain better insight into the effect of the native DNA environment on the IEs of the nucleobases, with the aid of the hybrid quantum mechanics/molecular mechanics (QM/MM) approach. The QM/MM approach consists of embedding a quantum mechanics calculation in a classical molecular mechanics model of the environment [65, 108]. The coupling between the QM region treated by quantum mechanics and the MM region treated with classical molecular mechanics must be able to describe both bonded and non-bonded interactions, such as electrostatic and van der Waals interactions, between the two regions. The use of the QM/MM approach allows thus to provide an explicit molecular description of the environmental effects taking into account the local structure of the solvent and the coordination of counterions in solution. This QM/MM approach has been used to computationally estimate the ionization energies of nucleobases within the biological environment showing the large effect on these properties [33]. The predicted energies are collected in Table 4 in which they are compared to the corresponding gas phase values. For the first time, the application of the QM/MM approach to the study of the ionization process of DNA shows how the negative phosphate groups of the DNA double helix and positive counterions induce a long-range molecular structure of the solvent creating, in the center of the DNA helix, a noticeably amplified electric potential. This potential shifts the ionization energy threshold of DNA bases by 3.2–3.3 eV relative to the gas phase. The QM/MM model has also been applied to IE calculations of clusters of DNA bases. The important IE shift due to solvation surrounding DNA remains at the same level as for single DNA bases. The results of this study have lead to detailed and reliable information about IEs of the DNA components providing a fundamental understanding of the electronic factors that influence site-specific or sequence-specific electron detachment on the genetic material.

7 A fruitful perspective

One of the main advantages of our group is a shared expertise dedicated to a wide range of problems. We plan to apply this advantage toward new perspectives. For example, one goal common to the three orientations of our respective research fields is to expand the size of the systems under study toward biological molecules, heavy atoms and ions, molecules containing transition metal atoms, molecular complexes or dynamics at ice surfaces. We will also approach the determination of new properties that will necessitate further theoretical developments, such as atomic and molecular photoionization cross-sections. Finally, we plan to carry on with the methodological transfers from electronic ab initio methods to nuclear dynamics (molecular vibration–rotation). All those projects are closely connected with experiments and will keep tightened all the members of the laboratory.

Acknowledgments SVe, CN, MD, and SVr are grateful to the "Fonds pour la formation la Recherche dans l'Industrie et dans l'Agriculture" of Belgium for a PhD grant (Boursier F.R.S.-FNRS). MG, JL, JGL, and NV thank the Communauté française of Belgium (Action de Recherche Concertée) and the Belgian National Fund for Scientific Research (FRFC/IISN Convention) for financial support.

References

1. Aboussaïd A, Godefroid M, Jönsson P, Froese Fischer C (1995) Phys Rev A 51:2031–9
2. Andrae D, Häussermann U, Dolg M, Stoll H, Preuss H (1990) Theor Chim Acta 77:123
3. Arnau A, Aumayr F, Echenique PM, Grether M, Heiland W, Limburg J, Morgenstern R, Roncin P, Schippers S, Schuch R, Stolterfoht N, Varga P, Zouros TJM, Winter HP (1997) Surf Sci Rep 27:113
4. Aumayr F, Kurz H, Schneider D, Briere MA, McDonald JW, Cunningham CE, Winter HP (1993) Phys Rev Lett 71:1943

5. Bacchus-Montabonel M-C, Vaeck N, Lasorne B, Desouter-Lecomte M (2003) Chem Phys Lett 374:307–313
6. Bader R (1994) Atoms in molecules: a quantum theory. Oxford University Press, USA
7. Baloïtcha E, Desouter-Lecomte M, Bacchus-Montabonel M-C, Vaeck N (2001) J Chem Phys 114:8741–51
8. Bartlett RJ (2010) Mol Phys 108(21–23):2905–2920
9. Bartlett RJ (2010) Mol Phys 108(21–23):3299–3311
10. Blondel C, Delsart C, Dulieu F (1996) Phys Rev Lett 77(18):3755–3758
11. Blondel C, Delsart C, Valli C, Yiou S, Godefroid M, Eck SV (2001) Phys Rev A 64:052504
12. Borgoo A, Scharf O, Gaigalas G, Godefroid M (2010) Comput Phys Commun 181:426–439
13. Borgoo A, Godefroid M, Geerlings P (2011) In: Hoggan P, Brändas E, Maruani J, Delgado-Barrio PPG (eds) Advances in the theory of quantum systems in chemistry and physics, progress in theoretical chemistry and physics, B22, chap 9, Springer, Dordrecht, pp 139–171
14. Boudon V, Pirali O, Roy P, Brubach J-B, Manceron L, Vander Auwera J (2010) J Quant Spectrosc Radiat Transfer 111: 1117–1129
15. Boys S, Bernardi F (1970) Mol Phys 19:553
16. Brage T, Froese Fischer C, Vaeck N, Godefroid M, Hibbert A (1993) Phys Scr 48:533–545
17. Brage T, Judge P, Aboussaïd A, Godefroid M, Froese Fischer C, Jönsson P, Ynnerman A, Leckrone D (1998) Astrophys J 500:507–521
18. Brage T, Judge PG, Proffitt CR (2002) Phys Rev Lett 89(28): 281101
19. Buijsse B, van der Zande JW, Eppink ATJB, Parker DH, Lewis RS, Gibson ST (1998) J Chem Phys 108:7229
20. Carette T, Drag C, Scharf O, Blondel C, Delsart C, Froese Fischer C, Godefroid M (2010) Phys Rev A 81:042522
21. Carette T, Nemouchi M, Jönsson P, Godefroid M (2010) Eur Phys J D 60:231–242
22. Carette T, Godefroid M (2011) Phys Rev A 83:062505
23. Carette T, Li J, Nemouchi M, Godefroid M (2012) Phys Rev A (work in progress)
24. Casado MA, Perez-Torrente JJ, Ciriano MA, Oro LA, Orejon A, Claver C (1999) Organometallics 18:3035–3044
25. Cassam-Chenaï P (2003) J Quant Spectrosc Radiat Transfer 82:251–277
26. Cassam-Chenaï P, Liévin J (2003) Int J Quantum Chem 93: 245–264
27. Cassam-Chenaï P, Liévin J (2006) J Comput Chem 27:627–640
28. Cassam-Chenaï P, Bouret Y, Rey M, Tashkun SA, Nikitin AV, Tyuterev VG (2012) Int J Quantum Chem 112:2201–2220
29. Cassam-Chenaï P, Liévin J (2012) J Chem Phys 136:174–309
30. Cauët E, Dehareng D, Liévin J (2006) J Phys Chem A 110(29):9200–9211
31. Cauët E, Liévin J (2007) Adv Quantum Chem 52:121–147
32. Cauët E, Liëvin J (2009) J Phys Chem A 113(36):9881–9890
33. Cauët E, Valiev M, Weare JH (2010) J Phys Chem B 114(17):5886–5894
34. Cauët E, Bogatko S, Mugeniwabagara E, Fusaro L, Kirsch-De Mesmaeker A, Luhmer M, Vaeck N (2010) Inorg Chem 49(17):7826–7831
35. Cauët E (2011) In: Marissa J, Campbell (eds) Quantum mechanical methods related to ionization of nucleic acid bases. Nova Publishers, New York
36. Cauët E (2011) J Biomol Struct Dyn 29(3):557–561
37. Cheung AS-C, Yoshino K, Parkinson WH, Guberman SL, Freeman DE (1986) Planet Space Sci 34:1007
38. Close DM (2004) J Phys Chem A 108(46):10376–10379
39. Close DM, Crespo-Hernández CE, Gorb L, Leszczynski J (2005) J Phys Chem A 109(41):9279–9283
40. Close DM, Crespo-Hernandez CE, Gorb L, Leszczynski J (2006) J Phys Chem A 110(23):7485–7490
41. Colin R, de Greef D, Goethals P, Verhaegen G (1974) Chem Phys Lett 25(1):70–73
42. Colson AO, Besler B, Sevilla MD (1993) J Phys Chem 97(51):13852–13859
43. Crespo-Hernández CE, Arce R, Ishikawa Y, Gorb L, Leszczynski J, Close DM (2004) J Phys Chem A 108(30): 6373–6377
44. Crespo-Hernandez CE, Close DM, Gorb L, Leszczynski J (2007) J Phys Chem B 111(19):5386–5395
45. Cumberland RW, Weinberger MB, Gilman JJ, Clark SM, Tolbert SH, Kaner RB (2005) J Am Chem Soc 127(20):7264–7265
46. Cunhade Miranda BK, Alcaraz C, Elhanine M, Noller B, Hemberger P, Fischer I, Garcia GA, Soldi-Lose H, Gans B, Vieira Mendes LA, Boyé-Péronne S, Douin S, Zabka J, Botschwina P (2010) J Phys Chem A 114:4818–4830
47. Delsaut M (2012) Ph.D. thesis, Université libre de Bruxelles (work in progress)
48. Deroo S, Le Gac S, Ghosh S, Villien M, Gerbaux P, Defrancq E, Moucheron C, Dumy P, Kirsch-De Mesmaeker A (2009) Eur J Inorg Chem 2009(4):524–532
49. Desclaux JP, Moser CM, Verhaegen G (1971) J Phys B At Mol Phys 4(3):296
50. Dian A (2002) PhD thesis, Université Libre de Bruxelles
51. Didriche K, Herman M (2010) Chem Phys Lett 496:1–7
52. Didriche K, Lauzin C, Foldes T, de Ghellinck D'Elseghem Vaernewijck X, Herman M (2010) Mol Phys 108:2155
53. Domcke WD (2011) In Domcke WD, Yarkoni DR, Köppel H (eds) Conical intersections. Theory, computation and experiment. Advanced series in physical chemistry, vol 17. World scientific Publishing Co, Singapore
54. Dunning T (1989) J Chem Phys 90:1007
55. Elias B, Kirsch-De Mesmaeker A (2006) Coordin Chem Rev 250(13–14):1627–1641
56. Fano U (1965) Phys Rev A 140:67–75
57. Feller D (1992) J Chem Phys 96:6104
58. Feyer V, Plekan O, Richter R, Coreno M, Vall-llosera G, Prince KC, Trofimov AB, Zaytseva IL, Moskovskaya TE, Gromov EV, Schirmer J (2009) J Phys Chem A 113(19):5736–5742
59. Folkerts L, Das J, Bergsma SW, Morgenstern R (1992) Phys Lett A 163:73
60. Froese Fischer C (1977) The Hartree–Fock method for atoms. A numerical approach. Wiley, New York
61. Froese Fischer C, Tachiev G, Gaigalas G, Godefroid M (2007) Comput Phys Commun 176:559–579
62. Gaardsted JO, Andersen T, Haugen HK, Hansen JE, Vaeck N (1991) J Phys B At Mol Phys 24:4363–4377
63. Gaidamauskas E, Nazé C, Rynkun P, Gaigalas G, Jönsson P, Godefroid M (2011) J Phys B At Mol Phys 44(17):175003
64. Gaigalas G, Froese Fischer C (1996) Comput Phys Commun 98:255–264
65. Gao J, Truhlar DG (2002) Annu Rev Phys Chem 53:467–505
66. Gibb EL, Van Brunt KA, Brittain SD, Rettig TW (2007) Astrophys J 660:1572
67. Godefroid M, Berger JJ, Verhaegen G (1976) J Phys B At Mol Phys 9(13):2181
68. Godefroid M, Liévin J, Metz JY (1987) J Phys B At Mol Phys 20:3283–96
69. Godefroid M, Liévin J, Metz JY (1991) Int J Quant Chem XL:243–264
70. Godefroid M, Jönsson P, Froese Fischer C (1998) Phys Scr T78:33–46

71. Godefroid M, Froese Fischer C, Jönsson P (2001) J Phys B At Mol Phys 34:1079–1104
72. Golubeva AA, Krylov AI (2009) Phys Chem Chem Phys 11(9):1303–11
73. Grabowski I, Lotrich V, Hirata S (2010) Mol Phys 108(21–23): 3313–22
74. Grant I (2006) Relativistic atomic structure. In: Drake GWF (ed) Atomic, molecular and optical physics handbook. American Institute of Physics, Woodbury, New York, pp 325–357
75. Grant I (2007) Relativistic quantum theory of atoms and molecules. Theory and computation. Atomic, optical and plasma physics. Springer, New York
76. Hansen J, Bentley M, van der Hart H, Lister G, Shen YT, Vaeck N (1993) Phys Scr T47:7–17
77. Hanus M, Ryjácek F, Kabelác M, Kubar T, Bogdan TV, Trygubenko SA, Hobza P (2003) J Am Chem Soc 125(25): 7678–7688
78. Hansen JE, Schraa O, Vaeck N (1992) Phys Scr T41:41–44
79. van der Hart HW, Vaeck N, Hansen JE (1994) J Phys B At Mol Phys 27:3489–3514
80. van der Hart HW, Vaeck N, Hansen JE (1995) J Phys B At Mol Phys 28:5207–5228
81. Helgaker T, Klopper W, Koch H, Noga J (1997) J Chem Phys 106:9639
82. Heller A (2000) Spiers memorial lecture. On the hypothesis of cathodic protection of genes. Faraday Discussions 116:1–13. http://dx.doi.org/10.1039/B006196O
83. Herman J, Mental J (1982) J Geophys Res 87:8967
84. Herman L, Ghosh S, Defrancq E, Mesmaekera AKD (2008) J Org Chem 21(7–8):670–681
85. Jennerich R, Keiser A, Tate D (2006) Eur Phys J D 40:81–89
86. Jenouvrier A, Coquart B, Mérienne MF (1986) J Quant Spectrosc Radiat Transfer 36:249
87. Jenouvrier A, Mérienne MF, Coquart B, Carleer M, Fally S, Vandaele AC, Hermans C, Colin R (1999) J Mol Struct 198:136
88. Johnston HS, Paige M, Yao F (1984) J. Geophys. Res. 89:11661
89. Johnson W (2010) Can J Phys 99:1–9
90. Jönsson P, He X, Froese Fischer C, Grant I (2007) Comput Phys Commun 177:597–622
91. Jönsson P, Carette T, Nemouchi M, Godefroid M (2010) J Phys B At Mol Phys 43:115,006
92. Jönsson P, Gaigalas G, Bieroń J, Froese Fischer C, Grant I (2012) Comput Phys Commun (submitted)
93. Kaner R, Gilman J (2010) Osmium diboride compounds and their uses. Patent US 7,645,308 B2
94. Kendall RA, Dunning TH Jr (1992) J Chem Phys 96:6796
95. Knowles PJ, Werner HJ (1992) Theor Chim Acta 84:95–103
96. Kostko O, Bravaya K, Krylov A, Ahmed M (2010) Phys Chem Chem Phys 12(12):2860–2872
97. Langhoff R, Davidson ER (1974) J Chem Phys 8:62
98. Lasorne B, Bacchus-Montabonel MC, Vaeck N, Desouter-Lecomte M (2004) J Chem Phys 120:1271–1278
99. Lauzin C, Didriche K, Macko P, Demaison J, Liévin J, Herman M (2009) J Phys Chem A 113:2359
100. Lauzin C, Didriche K (2011) Phys Chem Chem Phys 751:2359
101. Lauzin C, Cauët E, Demaison J, Herman M, Stoll H, Liévin J (2012) Mol Phys (submitted)
102. Lefèvre F, Forget F (2009) Nature 460:720–723
103. Le Gac S, Rickling S, Gerbaux P, Defrancq E, Moucheron C, Kirsch-De Mesmaeker A (2009) Angew Chem Int Ed 48(6): 1122–1125
104. Li J, Gaigalas G, Godefroid M (2012) Comput Phys Commun (work in progress)
105. Liévin J, Breulet J, Clercq P, Metz J (1982) Theor Chim Acta 61:513–537
106. Liévin J, Vaeck N (1990) Int J Quant Chem 62:521–541
107. Liévin J, Demaison J, Herman M, Fayt A, Puzzarini C (2011) J Chem Phys 134:064119
108. Lin H, Truhlar D (2007) Theor Chim Acta 117:185–199
109. Lindgren B, Olofsson G Astron (1980) Astrophysics 84:300–303
110. Loreau J, Sodoga K, Lauvergnat D, Desouter-Lecomte M, Vaeck N (2010) Phys Rev A 82:012708
111. Loreau J, Liévin J, Vaeck N (2010) J Chem Phys 133:114302
112. Loreau J, Liévin J, Palmeri P, Quinet P, Vaeck N (2010) J Phys B At Mol Phys 43:065101
113. Loreau J, Ryabchenko S, Dalgarno A, Vaeck N (2011) Phys Rev A 84:052720
114. Loreau J, Urbain X, Lecointre J, Vaeck N (2011) Phys Rev A 84:053412
115. Malmqvist PA (1986) Int J Quant Chem XXX:479–494
116. Marian CM (2007) J Phys Chem A 111(8):1545–1553
117. Mons M, Piuzzi F, Dimicoli I, Gorb L, Leszczynski J (2006) J Phys Chem A 110(38):10921–10924
118. Naviliat-Cuncic O (2012) Laboratoire de Physique Corpusculaire, U.d.C.B.N.: private communication
119. Nikitin AV, Rey M, Tyuterev VG (2011) Chem Phys 501:179
120. Ndong M, Bomble L, Sugny D, Justum Y, Desouter-Lecomte M (2007) Phys Rev A 76(4):043424
121. de Oliveira G, Martin JML, de Proft F, Geerlings P (1999) Phys Rev A 60(2):1034–1045
122. Olsen J, Godefroid M, Jönsson P, Malmqvist PA, Froese Fischer C (1995) Phys Rev E 52:4499–4508
123. Palmeri P, Quinet P, Zitane N, Vaeck N (2001) J Phys B At Mol Phys 34:4125–4139
124. Pellegrini P, Vranckx S, Desouter-Lecomte M (2011) Phys Chem Chem Phys 13:18864
125. Perrier S, Mugeniwabagara E, Kirsch-De Mesmaeker A, Hore PJ, Luhmer M (2009) J Am Chem Soc 131(34):12458–12465
126. Peterson KA, Figgen D, Goll E, Stoll H, Dolg M (2003) J Chem Phys 119:11113
127. Pieniazek PA, Krylov AI, Bradforth SE (2007) J Chem Phys 127(4):044317
128. Pieniazek PA, Bradforth SE, Krylov AI (2008) J Chem Phys 129(7):074104
129. Pirre M, Rigaud P, Huguenin D (1984) Geophys Res Lett 11:1199
130. Prat F, Houk KN, Foote CS (1998) J Am Chem Soc 120(4):845–846
131. Puzzarini C, Heckert M, Gauss J (2008) J Chem Phys 128: 194108
132. Ram RS, Liévin J, Bernath PF (1998) J Chem Phys 109: 6329–6337
133. Ram RS, Liévin J, Bernath PF (1999) J Chem Phys 111: 3449–3456
134. Ram RS, Liévin J, Bernath PF (1999) J Mol Spectrosc 197:133–146
135. Ram RS, Adam AG, Tsouli A, Liévin J, Bernath P (2000) J Mol Spectrosc 202:116
136. Ram RS, Adam A, Sha W, Tsouli A, Liévin J, Bernath PF (2001) J Chem Phys 114:3977–3987
137. Ram RS, Liévin J, Bernath PF (2009) J Mol Spectrosc 256
138. Reinhold E, Ubachs W (2005) Mol Phys 103:1329
139. Riley KE, Pitoňák M, Černý J, Hobza P (2010) J Chem Theory Comput 6(1):66–80
140. Rooman M, Liévin J, Buisine E, Wintjens R (2002) J Mol Biol 319(1):67–76
141. Rooman M, Cauët E, Liévin J, Wintjens R (2011) J Biomol Struct Dyn 28(6):949–953
142. Rothman LS, Gordon IE, Barbe A, Benner D Chris, Bernath PF, Birk M, Boudon V, Brown LR, Campargue A, Champion J-P, Chance K, Coudert LH, Dana V, Devi VM, Fally S, Flaud J-M, Gamache RR, Goldman A, Jacquemart D, Kleiner I, Lacome N,

Lafferty WJ, Mandin J-Y, Massie ST, Mikhailenko SN, Miller CE, Moazzen-Ahmadi N, Naumenko OV, Nikitin AV, Orphal J, Perevalov VI, Perrin A, Predoi-Cross A, Rinsland CP, Rotger M, Šimečková M, Smith MAH, Sung K, Tashkun SA, Tennyson J, Toth RA, Vandaele AC, Vander Auwera J (2009) J Quant Spectrosc Radiat Transfer 110:533–572
143. Saito I, Takayama M, Sugiyama H, Nakatani K, Tsuchida A, Yamamoto M (1995) J Am Chem Soc 117(23):6406–6407
144. Saito I, Takayama M, Sugiyama H, Nakamura T (1997) J Photochem Photobiol A 106(1–3):141–144
145. Saito I, Nakamura T, Nakatani K, Yoshioka Y, Yamaguchi K, Sugiyama H (1998) J Am Chem Soc 120(48):12686–12687
146. Saito I, Nakamura T, Nakatani K (2000) J Am Chem Soc 122(13):3001–3006
147. Sang C, Jiao Y, Sun Y, Gou B (2011) Eur Phys J D 64:203–207
148. Shabaev V, Artemyev A (1994) J Phys B At Mol Phys 27:1307–1314
149. Shardanand, Prasad Rao AD (1977) J Quant Spectrosc Radiat Transfer 17:433
150. Shukla M, Leszczynski (2006) J Chem Phys Lett 429(1–3): 261–265
151. Sodoga K, Loreau J, Lauvergnat D, Justum Y, Vaeck N (2009) Desouter-Lecomte M. Phys Rev A 80:033417
152. Soorkia S, Shafizadeh N, Liévin J, Gaveau MA, Pothier C, Mestdagh J-M, Soep B, Field RW (2011) J Phys Chem A 115:9620–9632
153. Šponer J, Jurečka P, Hobza P (2006) Computational studies of RNA and DNA. Springer, Berlin, pp 343–388
154. Šponer J, Riley KE, Hobza P (2008) Phys Chem Chem Phys 10(19):2595–2610
155. Sugiyama H, Saito I (1996) J Am Chem Soc 118(30):7063–7068
156. Sugny D, Bomble L, Ribeyre T, Dulieu O, Desouter-Lecomte M (2009) Phys Rev A 80(4):042325
157. Tao FM, Pan YK (1992) J Chem Phys 97:4989
158. Tate DA, Aturaliye DN (1997/09/1/) Phys Rev A 56:1844
159. Treadway CR, Hill MG, Barton JK (2002) Chem Phys 281(2–3):409–428
160. Trofimov AB, Schirmer J, Kobychev VB, Potts AW, Holland DMP, Karlsson L (2006) J Phys B At Mol Phys 39(2):305
161. Vaeck N, Hansen JE (1989) J Phys B At Mol Phys 22(20):3137
162. Vaeck N, Hansen JE (1991) J Phys B At Mol Phys 24:L469–L475
163. Vaeck N, Hansen JE (1992) J Phys B At Mol Phys 25:3613–3619
164. Vaeck N, Hansen JE (1992) Surf Sci 269(270):596–600
165. Vaeck N, Hansen JE (1992) J Phys B At Mol Phys 25:3613–3619
166. Vaeck N, Hansen JE (1992) J Phys B At Mol Phys 25:3267–3282
167. Vaeck N, Hansen JE (1995) J Phys B At Mol Phys 28:3523–3543
168. Vaeck N, Desouter-Lecomte M, Liévin J (1999) J Phys B At Mol Phys 32:409–428
169. Vaeck N, Bacchus-Montabonel M-C, Baloïtcha E, Desouter-Lecomte M (2001) Phys Rev A 63:042704
170. Vaeck N, Hansen JE, Palmeri P, Quinet P, Zitane N, Godefroid M, Fritzsche S, Kylstra N (2001) Phys Scr 2001(T95):68
171. Vaeck N, Kylstra N (2002) Phys Rev A 65:062502
172. Vana M, Aumayr F, Lemell C, Winter HP (1995) Int J Mass Spectrom Ion Proc 149(150):45
173. Varandas A (2007) J Chem Phys 127:114316
174. Verdebout S, Jönsson P, Gaigalas G, Godefroid M, Froese Fischer C (2010) J Phys B At Mol Phys 43:074017
175. Verdebout S, Rynkun P, Jönsson P, Gaigalas G, Godefroid M, Froese Fischer C (2012) J Phys B At Mol Phys (in preparation)
176. Vranckx S, Jaouadi A, Pellegrini P, Bomble L, Vaeck N, Desouter-Lecomte M (2012) Advances in atom and single molecule machines (submitted)
177. Wales D (2003) Energy Landscapes. With applications to clusters, biomolecules and glasses. Cambridge University Press, Cambridge
178. Wauters L, Vaeck N (1996) Phys Rev C 53:497–500
179. Wauters L, Vaeck N, Godefroid M, van der Hart H, Demeur M (1997) J Phys B At Mol Phys 30:4569–4589
180. Werner HJ, Knowles PJ (1988) J Chem Phys 89:5803–5814
181. Werner HJ, Knowles PJ, Knizia G, Manby FR, Schütz M, Celani P, Korona T, Lindh R, Mitrushenkov A, Rauhut G, Shamasundar KR, Adler TB, Amos RD, Bernhardsson A, Berning A, Cooper DL, Deegan MJO, Dobbyn AJ, Eckert F, Goll E, Hampel C, Hesselmann A, Hetzer G, Hrenar T, Jansen G, Köppl C, Liu Y, Lloyd AW, Mata RA, May AJ, McNicholas SJ, Meyer W, Mura ME, Nicklass A, O'Neill DP, Palmieri P, Pflüger K, Pitzer R, Reiher M, Shiozaki T, Stoll H, Stone AJ, Tarroni R, Thorsteinsson T, Wang M, Wolf A (2010) Molpro, version 2010.1, a package of ab initio programs. See http://www.molpro.net
182. Woon DE, Dunning TH Jr (1995) J Chem Phys 103:4572
183. Ye YJ, Jiang Y (2000) Int J Quant Chem 78(2):112–130
184. Yoshino K, Cheung AS-C, Esmond JR, Parkinson WH, Freeman DE, Guberman SL, Jenouvrier, Coquart B, Mérienne M-F (1988) Planet Space Sci 12
185. Yoshino K, Esmond JR, Cheung AS-C, Freeman DE, Parkinson WH (1992) Planet Space Sci 40:185
186. Yoshioka Y, Kitagawa Y, Takano Y, Yamaguchi K, Nakamura T, Saito I (1999) J Am Chem Soc 121(38):8712–8719
187. Zhou J, Kostko O, Nicolas C, Tang X, Belau L, de Vries MS, Ahmed M (2009) J Phys Chem A 113(17):4829–4832